Measuring the Fractal Dimension of Signals: Morphological Covers and Iterative Optimization

Petros Maragos, *Senior Member, IEEE*, and Fang-Kuo Sun, *Senior Member, IEEE*

Abstract—**Fractals can model many classes of time-series data. The fractal dimension is an important characteristic of fractals that contains information about their geometrical structure at multiple scales. The covering methods are a class of efficient approaches to measure the fractal dimension of an arbitrary fractal signal by creating multiscale covers around the signal's graph. In this paper we develop a general method that uses multiscale morphological operations with varying structuring elements to unify and extend the theory and digital implementations of covering methods. It is theoretically established that, for the fractal dimension computation, covering one-dimensional signals with planar sets is equivalent to morphologically transforming the signal by one-dimensional functions, which reduces the computational complexity from quadratic in the signal's length to linear. Then a morphological covering algorithm is developed and applied to discrete-time signals synthesized from Weierstrass functions, fractal interpolation functions, and fractional Brownian motion. Further, for deterministic parametric fractals depending on a single parameter related to their dimension, we develop an optimization method that starts from an initial estimate and iteratively converges to the true fractal dimension by searching in the parameter space and minimizing a distance between the original signal and all such signals from the same class. Experimental results are also provided to demonstrate the good performance of the developed methods.**

I. Introduction

FRACTALS are mathematical sets with a high degree of geometrical complexity that can model many natural phenomena, as Mandelbrot's pioneering work [19] has demonstrated. Examples include physical objects such as clouds, mountains, trees, and coastlines [19], [42], as well as image intensity signals that emanate from certain types of fractal surfaces [34]. Although the fractal images are the most popularized class of fractals, there are also numerous natural processes described by time-series measurements (e.g., noises with power spectrum $\propto 1/|\omega|^{\beta}$; econometric and demographic data; and pitch variations in music signals) that are fractals [19], [42]. The one-dimensional *signals* representing these measurements are fractals in the sense that their graph is a fractal set. Thus, modeling fractal signals is of great interest in signal processing.

A very important characteristic of fractals useful for their description and classification is their fractal dimension D. Intuitively, D measures the degree of their boundary fragmentation or irregularity over multiple scales. It makes meaningful the measurement of metric aspects of fractal curves, such as their length. Specifically, given a measure unit like a "yardstick" of length ϵ, the length $L(\epsilon)$ of a curve at scale ϵ is equal to the number of yardsticks that can fit sequentially along the curve times ϵ. For a fractal curve, $L(\epsilon)$ increases within limit when ϵ decreases and follows the (generally approximate) power law

$$L(\epsilon) \approx (\text{constant}) \cdot \epsilon^{1-D}, \qquad \text{as } \epsilon \to 0. \tag{1}$$

In this paper we deal with the problem of measuring the fractal dimension of real-valued "topologically one-dimensional" signals; i.e., signals with one argument, which for simplicity will be referred to as time t. We start in Section II with a brief survey of existing methods, some of which are general, whereas others apply only to special classes of parametric fractals. Section III focuses on the covering methods, a class of general and efficient approaches to compute the fractal dimension of arbitrary fractals. We unify and extend many of the current digital implementations (i.e., [8] and the one-dimensional analogs of [32], [37], [33]) of covering methods by using multiscale morphological erosions and dilation with varying structuring elements. (The erosions and dilations are the basic operators of morphological signal analysis [35], [24].) In addition, we prove a main theoretical result (Theorems 1 and 2 in Section III-A) that provides the theoretical framework underlying all these digital implementations. We shall refer to these unified algorithms as the morphological covering method. Although it was theoretically known before [7], [19], [35], [41], [8] that covering the graph of one-dimensional continuous-time signals by disks or similar planar sets can yield the fractal dimension of the signal's graph, all these approaches (except for the variation method in [8]) involved two-dimensional processing of the signal at multiple scales. Thus, for a N-sample N-level digital signal, these set-cover methods re-

Manuscript received February 6, 1990; revised January 6, 1992. The work of P. Maragos was supported by the NSF under Grant MIPS-86-58150 with matching funds from Bellcore, DEC, Sun, and Xerox, in part by TASC, and in part by the ARO Grant DAAL03-86-K-0171 to the Brown-Harvard-M.I.T. Center for Intelligent Control Systems.

P. Maragos is with the Division of Applied Sciences, Harvard University, Cambridge, MA 02138.

F.-K. Sun is with Reading Information Technology, Inc., Reading, MA 01867, and was with the Analytic Sciences Corporation, Reading, MA, while this work was being done.

IEEE Log Number 9203336.

quire a $O(N^2)$ computational complexity at each scale. In contrast, our theoretical results establish the fact that covering the signal's graph with properly chosen one-dimensional functions yields identical results but it involves one-dimensional processing of the signal. Hence, our approach reduces the original set-cover complexity from quadratic to linear, since for a N-sample signal the function-cover method has complexity $O(N)$ at each scale. In Section III-B we also describe a morphological covering algorithm for estimating the fractal dimension of discrete-time signals and apply it to three classes of fractal signals. Overall, the morphological approach is conceptually useful as a unifying theme and has several practical advantages. Specifically, it can be implemented very efficiently by using one-dimensional morphological filtering and can yield results that are invariant with respect to shifting the signal's domain and/or affine scaling of its dynamic range. The latter advantage makes the morphological covering method more robust than the box counting method in the digital case.

The morphological covering method applies to arbitrary signals; e.g., in [23] it was applied to measuring the short-time fractal dimension of speech signals. In this paper, for numerical comparisons, we test its performance by applying it to synthetic fractal signals depending on a few parameters that uniquely determine their fractal dimension. There are numerous classes of such parametric fractal signals and related algorithms for their synthesis. The three classes of parametric fractals used in this paper are the deterministic *Weierstrass* cosine functions (WCF's) [13], [19], [4], the deterministic *fractal interpolation* functions (FIF's) [1], [2], [16], and the random functions of *fractional Brownian motion* (FBM) [21], [19], all defined in Section II-B. These fractals have been used in a variety of applications. Specifically, there are many natural phenomena that can be modeled using such parametric fractals; e.g., see [19], [29]. In addition, the FBM and FIF's have proven to be valuable in computer synthesis of images of natural scenes [42], [2].

Although the performance of the morphological covering method is good for many cases, it can be further improved in the case of some parametric fractals. Specifically, in Section IV we present the second main contribution of this paper, which is both a very effective method (i.e., it yields practically zero estimation errors) to estimate fractal dimension and a new way of looking at this problem. It is somewhat restricted since it applies only to deterministic parametric fractals depending on a single parameter that is in one-to-one correspondence with their fractal dimension, but the large number of such parametric classes and their practical applicability motivates well our new method. Our basic idea is as follows: So far researchers start from an original fractal signal of true fractal dimension D, use various approaches to derive an estimate D^* of D, and are content if the estimation error $|D - D^*|$ is small. This criterion, however, does not reveal anything about how "close" the original fractal signal f is to some other fractal signal of true dimension D^*. In our approach, from an initial morphological estimate D^*, we synthesize the corresponding fractal function f^*. Then by searching in the parameter space D, we solve a nonlinear optimization problem, where a distance is iteratively minimized between the original f and each new iteratively synthesized f^*. The process terminates when we reach a minimum. We have theoretically proven the existence of such a global minimum for both the Weierstrass and fractal interpolation functions by using two types of distances: standard l_p metrics and a signal distance developed from the Hausdorff set metric. We call the above approach the iterative optimization method and demonstrate its excellent performance both theoretically and experimentally.

II. Preliminaries

In this section we review several "fractal dimensions," which are more or less capable of quantifying the degree of fragmentation of curves. We also define three classes of parametric fractals. General discussions on these topics can be found in [19], [2], [9].

A. General Methods

Let X be a nonempty compact subset of the real plane $\mathbb{R}^2$.

1) Hausdorff Dimension [14], [5], [6]: An ϵ-cover of X is any countable set collection $\mathcal{K}(\epsilon) = \{X_i: i = 1, 2, \cdots\}$ such that $X \subseteq \cup_i X_i$ and $0 < \text{diam}\,(X_i) \leq \epsilon$ for all i, where diam (X_i) is the largest distance between any two points of X_i. The δ-dimensional Hausdorff measure of X is defined as

$$\mathcal{H}_\delta(X) = \lim_{\epsilon \to 0} \left(\inf_{\mathcal{K}(\epsilon)} \left\{ \sum_i [\text{diam}\,(X_i)]^\delta \right\} \right). \tag{2}$$

There is a critical real number $D_H \geq 0$ such that $\mathcal{H}_\delta(X) = 0$ for $\delta > D_H$ whereas $\mathcal{H}_\delta(X) = \infty$ for $\delta < D_H$. This critical D_H is the Hausdorff dimension of X. Mandelbrot [19] defines formally the *fractal dimension of X* as equal to D_H. Further, he calls a set *fractal* if D_H strictly exceeds its topological dimension D_T.

Two other dimensions, closely related to D_H, are the Minkowski–Bouligand dimension D_M and the box dimension D_B, which are identical in the continuous case. In general, we have

$$0 \leq D_T \leq D_H \leq D_M = D_B \leq 2.$$

To simplify the discussion on these two dimensions, we henceforth restrict our attention only to sets $X \subseteq \mathbb{R}^2$ that are continuous planar curves; hence, $1 \leq D_H \leq D_M \leq 2$.

2) Minkowski–Bouligand Dimension [30], [7]: This is based conceptually on Minkowski's idea of finding the length of irregular curves: Dilate them with disks of radius ϵ by forming the union of these disks centered at all points of X and thus create a "Minkowski cover." (Some [7], [19] attribute this cover construction also to Cantor.) Find the area $A(\epsilon)$ of the dilated set at all scales ϵ, and set

its length equal to $\lim_{\epsilon \to 0} L(\epsilon)$, where $L(\epsilon) = A(\epsilon)/2\epsilon$. See also [35, ch. 5] for a related discussion. If X is a fractal, then L behaves as in (1). Specifically, let

$$\lambda(A) \triangleq \sup \{ p: \lim_{\epsilon \to 0} A(\epsilon)\epsilon^{-p} = 0\} \tag{3}$$

$$= \lim_{\epsilon \to 0} \frac{\log A(\epsilon)}{\log \epsilon} \tag{4}$$

be the infinitesimal order[1] of A. Bouligand defined the dimension D_M as follows:

$$D_M = 2 - \lambda(A) \tag{5}$$

$$= \lim_{\epsilon \to 0} \left(2 - \frac{\log [A(\epsilon)]}{\log (\epsilon)} \right). \tag{6}$$

3) Box Counting Dimension [7]: Partition the plane with a grid of squares of side ϵ and count the number $N(\epsilon)$ of squares that intersect the curve. Then the box dimension is obtained by replacing the Minkowski cover area in (6) with the box cover area $\epsilon^2 N(\epsilon)$; it is equal to $D_B = \lim_{\epsilon \to 0} \log [N(\epsilon)]/\log (1/\epsilon)$. Although $D_B = D_M$ in the continuous case, they obviously correspond to two different algorithms (with different performances) in the discrete case. In general, D_M can be more robustly estimated than D_B, which suffers from uncertainties due to the grid translation or its spacing. This is further explained in Section III-B.

4) Entropy Dimension [17]: This dimension is defined as $D_E = \lim_{\epsilon \to 0} \log [N_{\min}(\epsilon)]/\log (1/\epsilon)$, where $N_{\min}(\epsilon)$ is the smallest number of disks with radii ϵ required to cover X. (It is also called the "capacity" dimension in [10].) In [2], [9] it is shown that $D_E = D_B$.

In general, $D_H \neq D_M = D_B$ [20], [28], [2], [9]. However, in this paper we focus on the Minkowski–Bouligand dimension D_M, which we shall henceforth call "fractal dimension" D because: i) it is closely related to D_H and hence able to quantify the fractal aspects of a signal; ii) it coincides (in the continuous case) with D_H in many cases of practical interest; iii) it is much easier to compute than D_H; iv) it is more robust to compute than D_B; v) it will be applied to discrete-time signals where most approaches can yield only approximate results.

B. Parametric Fractals

In this section we briefly describe the three classes of parametric fractal test signals on which we shall evaluate the various methods.

1) Weierstrass Cosine Function: The Weierstrass cosine function (WCF) [13], [19], [4] is defined as

$$W_H(t) = \sum_{k=0}^{\infty} \gamma^{-kH} \cos (2\pi\gamma^k t), \qquad 0 < H < 1 \tag{7}$$

where $\gamma > 1$. It is continuous but nowhere differentiable. Its fractal dimension is $D = 2 - H$. If γ is integer, then it is periodic with period one. In our experiments, we synthesized discrete-time signals from WCF's by sampling $t \in [0, 1]$ at $N + 1$ equidistant points, using a fixed $\gamma = 5$, and truncating the infinite series so that the summation is done only for $0 \leq k \leq k_{\max}$.[2] This causes a truncation error

$$\left| W_H(t) - \sum_{k=0}^{k_{\max}} \gamma^{-kH} \cos (2\pi\gamma^k t) \right| \leq \frac{\gamma^{-H(k_{\max}+1)}}{1 - \gamma^{-H}}. \tag{8}$$

Fig. 1(a) shows three sampled WCFs whose fragmentation increases with their dimension D.

2) Fractal Interpolation Functions: First, we summarize basic ideas from the theory of fractal interpolation functions [1], [2], [16]. Given is a set of data points $\{(x_k, y_k) \in \mathbb{R}^2; k = 0, 1, 2, \cdots, K > 1\}$ on the plane, where $x_{k-1} < x_k$ for all k. In the complete metric space $\mathcal{Q}$ of all continuous functions q: $[x_0, x_K] \to \mathbb{R}$ such that $q(x_0) = y_0$ and $q(x_K) = y_K$ define the function mapping Ψ by

$$\Psi(q)(x) = c_k \left(\frac{x - b_k}{a_k} \right) + V_k q \left(\frac{x - b_k}{a_k} \right) + d_k, \qquad x \in [x_{k-1}, x_k] \tag{9}$$

where $k = 1, 2, \cdots, K$, the $V_k \in (-1, 1)$ are free parameters, and the $4K$ parameters a_k, b_k, c_k, d_k are uniquely determined by

$$a_k x_0 + b_k = x_{k-1}, \qquad a_k x_K + b_k = x_k \tag{10}$$

$$V_k y_0 + c_k x_0 + d_k = y_{k-1}, \qquad V_k y_K + c_k x_K + d_k = y_k. \tag{11}$$

Under the action of Ψ the graph of the input function q is mapped to the graph of the output $\Psi(q)$ via affine mappings $(x, y) \mapsto (ax + b, Vy + cx + d)$, which include contractions and shifts of the domain and range of q. Ψ is a contraction mapping in $\mathcal{Q}$ and has a unique fixed point which is a continuous function F: $[x_0, x_K] \to \mathbb{R}$ that interpolates the given data; i.e., $F(x_k) = y_k$ for $k = 0, 1, \cdots, K$. F is called a fractal interpolation function (FIF),[3] because quite often the fractal dimension D of its graph exceeds 1. Specifically, [2], [12], if $\Sigma_{k=1}^{K} |V_k| > 1$ and (x_k, y_k) are not all collinear, then D is the unique real solution of

$$\sum_{k=1}^{K} |V_k| a_k^{D-1} = 1. \tag{12}$$

Otherwise, $D = 1$. Thus by choosing the vertical scaling ratios V_k's we can synthesize a fractal interpolation function of any desired fractal dimension. F can be synthesized by iterating Ψ on any initial function q in $\mathcal{Q}$; i.e., F $\lim_{n \to \infty} \Psi^{\circ n}(q)$ where $\Psi^{\circ n}(q) = \Psi[\Psi^{\circ (n-1)}(q)]$.

Given a finite-length discrete-time signal $f_o[k]$, $k = 0, 1, \cdots, K$, an algorithm was described in [23] to frac-

[1]For example, if X is a linear segment of length l, then $A(\epsilon) = 2l\epsilon + \pi\epsilon^2$ and $\lambda = 1$.

[2]The $k_{\max}$ was determined by requiring that $2\pi\gamma^k \leq 10^{12}$, because larger k caused an argument for the cosine that exceeded the (Sun4) computer's double precision.

[3]In [2], [27] more general FIF's are also discussed using hidden variables. In this paper we do not deal with these more general FIF's.

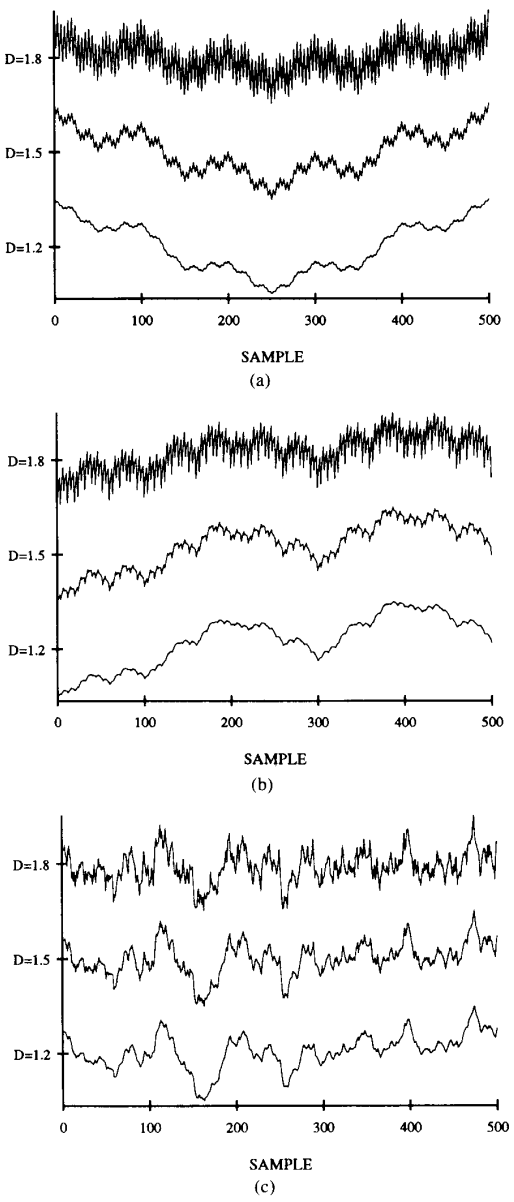

Fig. 1. (a) Signals from sampling WCF's over [0, 1] with $\gamma = 5$ and various D. (b) Signals from sampling FIF's that interpolate the sequence 0, 1, 4, 2, 5, 3 with various D. (c) FBM signals obtained via a 512-point inverse FFT on random spectra with average magnitude $\propto |\omega|^{D-2.5}$. (All three signals in each class have $N = 500$ and are scaled to have the same amplitude range.)

tally interpolate f_o by an integer factor M by sampling a FIF whose fractal dimension can be controlled via a single parameter. Specifically, we start from the $K + 1$ data pairs $(x_k = kM, y_k = f_o[k])$ with $x_K = MK = N$, set $a_k = 1/K$, $b_k = x_{k-1}$, and select a constant $V_k = V \in (-1, 1)$, where

$$|V| = K^{D-2}, \qquad 1 < D < 2. \tag{13}$$

Then there is a unique fractal interpolation function F_D: $[0, N] \rightarrow \mathbb{R}$ with fractal dimension D, which interpolates the given data, i.e., $F_D(kM) = f_o[k]$. In our experiments we synthesize F_D by iterating Ψ starting from some initial $q \in \mathcal{Q}$ until the maximum absolute error between successive iterations becomes very small, i.e., smaller than 10^{-10}. If $V = 0$, F_D is the piecewise-linear interpolant of the data. The graph of F_D has fractal dimension $D = 2 + \log(|V|)/\log(K)$ if $1 > |V| > 1/K$, and $D = 1$ if $|V| \leq 1/K$. Based on F_D we can up-sample f_o to a 1: M interpolated signal $F_D(n)$, $n = 0, 1, \cdots, N$. The larger $|V|$, the larger D, and the more fragmented F_D. Fig. 1(b) shows examples of FIF's that interpolate a fixed data sequence of $K + 1 = 6$ points by a factor $M = 100$ using positive ratios $V = 5^{D-2}$.

3) Fractional Brownian Motion: The fractional Brownian motion (FBM) [21], [19] $B_H(t)$ with parameter $0 < H < 1$ is a time-varying random function with stationary, Gaussian-distributed, and statistically self-affine increments; the latter means that $[B_H(t + T) - B_H(t)]$ is statistically indistinguishable from $r^{-H}[B(t + rT) - B(t)]$ for any T and any $r > 0$. The fractal dimension D of $B_H(t)$ is $D = 2 - H$. Their power spectrum[4] is $S_{\text{FBM}}(\omega) \propto 1/|\omega|^{2H+1}$. Hence, an efficient algorithm [42] to synthesize an FBM is to create a random sampled spectrum whose average magnitude is $1/|\omega|^{H+0.5}$ and its random phase is uniformly distributed over $[0, 2\pi]$. In our experiments we synthesized and then transformed this spectrum via an inverse FFT to obtain an FBM sequence from which we retained the first $N + 1$ samples. Fig. 1(c) shows synthesized FBM sequences of varying D. The larger D (the smaller H), the more fragmented these fractal signals look.

In addition to the FFT method, there are several other methods to synthesize FBM signals [22], [42]. One rigorous approach discussed in [18] involves Cholesky decomposition of the correlation matrix of discrete fractional Gaussian noise (i.e., sequence of increments of FBM) and synthesizing the FBM as a running average of the fractional noise. This approach, however, is computationally more complex than the FFT approach.

C. Special Methods for FBM

Some special methods to measure D for FBM signals include: i) Fitting a straight line to the data ($\log S_{\text{FBM}}(\omega)$, $\log \omega$) and measuring the slope yields D. This is perhaps the most popular method because of the simplicity of computing spectra using FFT. The power spectrum estimation part of this approach has been improved in various ways which include using Gabor filters (for two-dimensional FBM) in [39] and wavelet decomposition of $1/|\omega|^{\beta}$ processes in noise [43]. ii) The statistical self-affinity of FBM yields a power scaling law for many of its moments; linear regression on these data can measure D [34]. iii) Maximum likelihood methods for estimating the H of

[4]Strictly speaking, the power spectrum of the nonstationary FBM is not well defined. However, for $\omega \neq 0$, we can approximately interpret $S_{\text{FBM}}(\omega)$ as proportional to the average power of FBM within a narrow frequency band around ω [19].

fractional Gaussian noise have been developed in [18] and [40].

III. Morphological Covering Method

A. Morphological Covers

In this paper we deal only with finite-length signals $f(t)$, $0 \le t \le T$, in which case the curve X of the previous discussion becomes the graph $\Gamma(f) = \{(t, f(t)): 0 \le t \le T\}$ of f. If (x, y) are the Cartesian coordinates of the plane $\mathbb{R}^2$, the time t axis will henceforth coincide with the x axis, whereas the signal amplitude $f(t)$ assumes values on the y axis. In this section we shall focus on a generalized version of the Minkowski cover method. Bouligand [7] showed that D_M can be obtained by also replacing the disks or the boxes in the previous covers with arbitrarily shaped compact sets that possess a nonzero minimum and maximum distance from their center to their boundary. A very similar method appeared recently in Tricot *et al.* [41] and Dubuc *et al.* [8].

We formalize Bouligand's idea using morphological operations as follows: Given a compact planar set $B \subseteq \mathbb{R}^2$, form positive homothetics $\epsilon B = \{\epsilon b: b \in B\}$, and define the cover $C_B(\epsilon)$ as the union of all vector translates $\epsilon B + z = \{\epsilon b + z; b \in B\}$ of ϵB centered at points z of the graph $\Gamma(f)$. In the formalism of mathematical morphology, this cover can be obtained from the set dilation $\oplus$ of $\Gamma(f)$ by the set structuring element ϵB:

$$C_B(\epsilon) \triangleq \Gamma(f) \oplus \epsilon B = \cup_{z \in \Gamma(f)} \epsilon B + z = \{(t + x, f(t) + y): (t, f(t)) \in \Gamma(f), (x, y) \in \epsilon B\}. \quad (14)$$

Henceforth we call C_B a morphological cover. The Minkowski cover corresponds to using a disk for B.

In [41], [8] the digital implementations of the covering by disk-like or other (e.g., horizontal line segment) structuring elements were done by viewing $\Gamma(f)$ as a binary image signal and dilating this binary image. However, this two-dimensional processing of a one-dimensional signal, on the one hand is unnecessary, and on the other hand increases the requirements in storage space and the time complexity for implementing the covering method. Thus, for purposes of computational efficiency, it is desirable to obtain the area of C_B by using one-dimensional operations on f, i.e., dilations $\oplus$ and erosions $\ominus$ of f by a function structuring element g with a compact support G. These operations (see [35], [38], [24], [25], [11], [15], [36] for more details and their properties) are defined as

$$(f \oplus g)(t) \triangleq \sup_{x \in \check{G} + t} \{f(x) + g(t - x)\}, \quad t \in \mathbb{R} \quad (15)$$

$$(f \ominus g)(t) \triangleq \inf_{x \in G + t} \{f(x) + g(x - t)\}, \quad t \in \mathbb{R} \quad (16)$$

where $\check{G} = \{-x: x \in G\}$ is the reflection of G and $G + t = \{x + t; x \in G\}$ is the translation of G by t. Also, we set $f(t) = -\infty$ for $t \notin [0, T]$ and $g(t) = -\infty$ for $t \notin G$. Then, under certain assumptions (discussed later), we could obtain the cover area by integrating the difference signal $f \oplus g - f \ominus g$. However, since f is defined only over $[0, T]$ and the morphological cover C_B involves points t from outside this interval, we modify the cover and the signal operations $f \oplus g$, $f \ominus g$ to handle the boundaries of f properly. Thus, we replace the covers $C_B(\epsilon)$ with their restriction on the vertical strip $[0, T] \times (-\infty, \infty)$, i.e., with the *truncated* morphological cover

$$C_B^*(\epsilon) \triangleq [\Gamma(f) \oplus \epsilon B] \cap ([0, T] \times (-\infty, \infty)) \quad (17)$$

whose area is

$$A_B(\epsilon) \triangleq \text{area } [C_B^*(\epsilon)]. \quad (18)$$

To obtain A_B from one-dimensional dilations and erosions, we should also modify the definitions (15) and (16) so that they do not require any values of f outside $[0, T]$. Thus, we define the *support-limited* dilation and erosion of f by g with respect to a support set $S \subseteq \mathbb{R}$:

$$(f \oplus_S g)(t) \triangleq \sup_{x \in (\check{G} + t) \cap S} \{f(x) + g(t - x)\}, \quad t \in S \quad (19)$$

$$(f \ominus_S g)(t) \triangleq \inf_{x \in (G + t) \cap S} \{f(x) + g(x - t)\}, \quad t \in S. \quad (20)$$

In what follows we shall find a proper g such that the integral of the difference signal between the support-limited dilation and the erosion of f by g is equal to the original set-cover area $A_B(\epsilon)$ at all scales ϵ, if B satisfies certain constraints. The following theorem provides the main theoretical result toward this goal and illuminates the individual steps for constructing such a g.

Theorem 1: Let $f: S \to \mathbb{R}$ be a continuous function, where $S = [0, T]$. Let $B \subseteq \mathbb{R}^2$ be a compact set that is also single connected (i.e., connected with no holes) and symmetric with respect to both the x and the y axes of the plane.[5] For each scale $\epsilon \ge 0$, the "upper and lower envelope" of the morphological cover $C_B^*(\epsilon)$ are defined, respectively, as the signals

$$U_\epsilon(x) \triangleq \sup \{y: (x, y) \in C_B^*(\epsilon)\} \quad (21)$$

$$L_\epsilon(x) \triangleq \inf \{y: (x, y) \in C_B^*(\epsilon)\}. \quad (22)$$

Then,

$$A_B(\epsilon) = \int_0^T [U_\epsilon(x) - L_\epsilon(x)]\, dx. \quad (23)$$

Further, if we define a function

$$g(x) \triangleq \sup \{y: (x, y) \in B\} \quad (24)$$

[5]It is simple to generalize our results by allowing B to be asymmetric with respect to the x axis, which would mean that our covers would not be symmetric above and below the graph of the signal. We could also allow B to be asymmetric with respect to the y axis, which would mean that g is not an even function and hence treats differently signal segments in the past from those in the future of some point. However, both of these generalizations lack a practical motivation.

and its ϵ-scaled version by

$$g_\epsilon(x) \triangleq \sup\{y: (x, y) \in \epsilon B\}, \qquad \epsilon \geq 0 \tag{25}$$

then

$$\begin{aligned} U_\epsilon(x) &= f \oplus_S g_\epsilon(x) \\ L_\epsilon(x) &= f \ominus_S g_\epsilon(x) \end{aligned} \qquad 0 \leq x \leq T. \tag{26}$$

Thus, if we define the function-cover area

$$A_g(\epsilon) \triangleq \int_0^T [(f \oplus_S g_\epsilon) - (f \ominus_S g_\epsilon)](x)\, dx \tag{27}$$

then the set-cover and function-cover areas are identical:

$$A_B(\epsilon) = A_g(\epsilon). \tag{28}$$

Proof: Let $G = \{x: (x, y) \in B\}$. Since B is symmetric with respect to the y axis, $g_\epsilon(x) = g_\epsilon(-x)$ and $G = \check{G}$. Since B is symmetric with respect to the x axis, $g_\epsilon(x) \geq 0$ for all x in its domain ϵG. If $I(a) = \{b: (a, b) \in \epsilon B\}$ for any $a \in \epsilon G$, then note that $\sup\{b: b \in I(a)\} = g_\epsilon(a)$ and $\inf\{b: b \in I(a)\} = -g_\epsilon(a)$. To prove (26) we have, for each $x \in S$,

$$\begin{aligned} U_\epsilon(x) &= \sup\{y: y = f(t) + b, t \in S, x = t + a, \\ &\qquad (a, b) \in \epsilon B\} \\ &= \sup\{f(x - a) + b: \\ &\qquad a \in \epsilon G \cap (\check{S} + x), b \in I(a)\} \\ &= \sup\{f(t) + g_\epsilon(x - t): x \in S \cap (\epsilon G + t)\} \\ &= (f \oplus_S g_\epsilon)(x). \end{aligned}$$

Likewise we can prove that $L_\epsilon = f \ominus_S g_\epsilon$.

Since $g_\epsilon(0) \geq 0$, it can be easily shown that

$$U_\epsilon(x) \geq f(x) \geq L_\epsilon(x), \qquad 0 \leq x \leq T.$$

Let $\mathfrak{F}(\epsilon) = \{(x, y): 0 \leq x \leq T, L_\epsilon(x) \leq y \leq U_\epsilon(x)\}$. We shall prove that $\mathfrak{F}(\epsilon) = C_B^*(\epsilon)$. First, let $(x, y) \in C_B^*(\epsilon)$. Then, $x \in S$ and $(x, y) \in \Gamma(f) \oplus \epsilon B$. Hence, $x = t + a$, and $y = f(t) + b$ for some $t \in S$ and $(a, b) \in \epsilon B$. But then, from the definition of U_ϵ, it follows that $y \leq U_\epsilon(x)$; likewise, $y \geq L_\epsilon(x)$. Therefore, $(x, y) \in \mathfrak{F}(\epsilon)$ and thus $C_B^*(\epsilon) \subseteq \mathfrak{F}(\epsilon)$.

Now let $(x, y) \in \mathfrak{F}(\epsilon)$. We shall prove that $(x, y) \in C_B^*(\epsilon)$. Define the set $\mathcal{K} = \{(a, b): a \in \epsilon G \cap (\check{S} + x), b \in I(a)\}$. Then $\mathcal{K} = \epsilon B \cap [(\check{S} + x) \times (-\infty, +\infty)]$ is a connected set. Define the function $\phi(a, b) = f(x - a) + b$ on $\mathcal{K}$. The function ϕ is continuous and has a connected domain $\mathcal{K}$. The value y lies between the maximum $U_\epsilon(x) = \sup\{\phi(a, b): (a, b) \in \mathcal{K}\}$ and the minimum $L_\epsilon(x) = \inf\{\phi(a, b): (a, b) \in \mathcal{K}\}$ value of ϕ on $\mathcal{K}$. Hence, from Bolzano's intermediate value theorem [3, p. 153], there is a point (a', b') in $\mathcal{K}$ at which ϕ takes the value y. By setting $t = x - a'$ and $f(t) = y - b'$ we have $(t, f(t)) \in \Gamma(f)$ and $(a', b') \in \epsilon B$. Hence $(x, y) \in C_B^*(\epsilon)$ and thus $\mathfrak{F}(\epsilon) \subseteq C_B^*(\epsilon)$. Therefore, we proved that $\mathfrak{F}(\epsilon) = C_B^*(\epsilon)$. This set equality proves (23). The result $A_B = A_g$ follows from (23) and (26). Thus the proof is complete. □

Thus, instead of creating the cover of a one-dimensional signal by dilating its graph in the plane by a set B (which means two-dimensional processing), the original one-dimensional signal can be filtered with an erosion and a dilation by a one-dimensional function g. As an example, if $B = \{(x, y): x^2 + y^2 \leq 1\}$ is the unit-radius disk, then $g(x) = \sqrt{1 - x^2}$, $|x| \leq 1$. Likewise, if $B = \{(x, y): |x| + |y| \leq 1\}$ is the unit rhombus, then $g(x) = 1 - |x|$, $|x| \leq 1$.

In a related work, Tricot *et al.* [41] and Dubuc *et al.* [8] showed that we can find D_M by using set covers where B is the horizontal segment $[-1, 1]$ and that

$$v(\epsilon) \triangleq \int_0^T \left[\sup_{|y| \leq \epsilon}\{f(x + y)\} - \inf_{|y| \leq \epsilon}\{f(x + y)\}\right] dx \tag{29}$$

which is called the "variation" of f, is equal to $A_B(\epsilon)$ if $B = [-1, 1]$. Their result becomes a special case of our Theorem 1. Specifically, the assumptions of Theorem 1 allow for B to be equal to intervals $[-w, w]$, in which case $g(t) = 0$ for $t \in B$ and $g(t) = -\infty$ for $t \notin B$. Thus the horizontal structuring element case corresponds to selecting a function g shaped like a rectangle and equal to zero on its support.

The following theorem shows that we can find the fractal dimension D_M of the signal's graph by using covers with functions g.

Theorem 2: Let the function f and set B satisfy all the assumptions of Theorem 1. If B has any of the following two additional properties: a) B contains the origin and possesses a nonzero minimum distance from the origin to its boundary, or b) B is a horizontal segment $[-w, w]$, $w > 0$, then the Minkowski–Bouligand dimension of the graph of f is equal to

$$D_M = 2 - \lambda(A_g) \tag{30}$$

$$= \lim_{\epsilon \to 0}\left(2 - \frac{\log[A_g(\epsilon)]}{\log(\epsilon)}\right). \tag{31}$$

Proof: a) Bouligand [7] showed that D_M remains unchanged if we replace the area A of the cover by disks in (6) with the area of covers C_B by compact sets B that possess a nonzero minimum (m) and maximum (M) distance from the origin to their boundaries. Now the area of $C_B(\epsilon)$ is equal to the area $A_B(\epsilon)$ of the truncated cover $C_B^*(\epsilon)$ plus the term area(ϵB) because half of ϵB is added at each boundary of f. However, $\lambda[\text{area}(\epsilon B)] = 2$ because

$$\pi(m\epsilon)^2 \leq \text{area}(\epsilon B) \leq \pi(M\epsilon)^2.$$

Hence, since $\lambda(A_B) = 2 - D_M \leq 1$, we can ignore the term area(ϵB) and use as cover areas in (6) the areas A_B of the truncated covers. Then, Theorem 1 completes the proof, since it allows replacing the area of covers by sets with the area of covers by functions.

b) A proof for the special case $B = [-1, 1]$ appeared in [41], [8]. Thus, if $A_1(\epsilon)$ is the cover area of f by the set $[-1, 1]$, then $\lambda(A_1) = 2 - D_M$. For the more general

case $B = [-w, w]$, note that $A_B(\epsilon/w) = A_1(\epsilon)$, $w > 0$. Then,

$$\lambda(A_1) = \lim_{\epsilon \to 0} \frac{\log [A_B(\epsilon/w)]}{\log (\epsilon)} = \lim_{\epsilon \to 0} \frac{\log [A_B(\epsilon/w)]}{\log (\epsilon/w)} \cdot \frac{\log (\epsilon/w)}{\log (\epsilon)} = \lambda(A_B).$$

Hence, $D_M = 2 - \lambda(A_B)$. Then result (28) completes the proof of b). □

In practice, assuming that $A_g(\epsilon) \approx$ (constant) $\cdot \epsilon^{\lambda}$ for ϵ very close to 0 yields that

$$\log \frac{A_g(\epsilon)}{\epsilon^2} \approx D_M \cdot \log \left(\frac{1}{\epsilon}\right) + \text{constant}, \qquad \text{as } \epsilon \to 0. \tag{32}$$

This leads to the following practical algorithm to compute D_M in the discrete case.

B. Algorithm for Discrete-Time Signals

The goal here is to adapt our discussion in Section III-A for estimating the fractal dimension of a continuous-time signal to the case of a discrete-time finite-length signal $f[n]$, $n = 0, 1, \cdots, N$ by using covers at discrete scales $\epsilon = 1, 2, 3, \cdots, \epsilon_{\max}$. Toward this goal we put another restriction on B, that it must be *convex* for the following reason. In [2], if B is convex and $\epsilon = 0, 1, 2, \cdots$, then $\epsilon B = B^{\oplus \epsilon}$ where $B^{\oplus \epsilon} = B \oplus B \cdots \oplus B$ (ϵ times). Hence, for B convex and integer ϵ, g_ϵ is equal to $g^{\oplus \epsilon} \triangleq g \oplus g \cdots \oplus g$, i.e., the ϵ-fold dilation of g with itself. Then it can be shown that

$$f \oplus_S g^{\oplus \epsilon} = ((f \oplus_S g) \oplus_S g \cdots) \oplus_S g \tag{33}$$

$$f \ominus_S g^{\oplus \epsilon} = \underbrace{((f \ominus_S g) \ominus_S g \cdots) \ominus_S g}_{\epsilon \text{ times}}. \tag{34}$$

Hence the quadratic complexity (with respect to the maximum scale $\epsilon_{\max}$) of computing the covers at all scales ϵ can be reduced to linear.

Putting all the above ideas together leads to the following algorithm for digitally implementing the morphological covering method. This consists of the following steps:

Step 1: Select a set structuring element B to be a discrete version of a continuous set B_c that satisfies the assumptions of Theorems 1 and 2a) or 1 and 2b) and is convex. Preferably this set should have a "radius" one in both x and y directions. (Larger integer radii would yield cover area measurements over a coarser set of scales.) That is, B should be a convex symmetric subset of the 3 $\times$ 3 square set of points from the rectangular grid of pixels (n, mh) where (n, m) are integer coordinates and h is the vertical grid spacing. Then $g[n]$, $n = -1, 0, 1$, is a three-sample function whose graph is the upper envelope of B. There are only three choices for such a unit-radius B: the 3 $\times$ 3 pixel square, the 5-pixel rhombus, and the 3-pixel horizontal segment.

i) If B is the 3 $\times$ 3-pixel square, the corresponding g is shaped like a rectangle; i.e.,

$$g_r[-1] = g_r[0] = g_r[1] = h \geq 0 \tag{35}$$

and $g_r[n] = -\infty$ for $n \neq -1, 0, 1$.

ii) If B is the 5-pixel rhombus, then g is shaped like a triangle, defined by

$$g_t[-1] = g_t[1] = 0, \; g_t[0] = h \geq 0 \tag{36}$$

and $g_t[n] = -\infty$ for $n \neq -1, 0, 1$.

iii) If B is the 3-pixel horizontal segment, then the corresponding g can be viewed as resulting either from g_t or from g_r by setting $h = 0$. In this case g is a rectangular function equal to zero on its support.

Step 2: Perform recursively the support-limited dilations and erosions of f by $g^{\oplus \epsilon}$ at scales $\epsilon = 1, 2, \cdots, \epsilon_{\max}$. That is, set $G = \{-1, 0, 1,\}$, $S = \{0, 1, \cdots, N\}$, and use (19) and (33), which yield

$$f \oplus_S g[n] = \max_{-1 \leq i \leq 1} \{f[n + i] + g[i]\}, \qquad \epsilon = 1$$

$$f \oplus_S g^{\oplus(\epsilon+1)} = (f \oplus_S g^{\oplus \epsilon}) \oplus_S g, \qquad \epsilon \geq 2. \tag{37}$$

Likewise for the erosions $f \ominus_S g^{\oplus \epsilon}$. For $n = 0, N$, the local max/min operations take place only over the available samples. The dashed lines in Fig. 2 show these multiscale erosions/dilations by the three different functions g.

Step 3: Compute the cover areas

$$A_g[\epsilon] = \sum_{n=0}^{N} ((f \oplus_S g^{\oplus \epsilon}) - (f \ominus_S g^{\oplus \epsilon}))[n], \qquad \epsilon = 1, \cdots, \epsilon_{\max} \leq \frac{N}{2}. \tag{38}$$

Step 4: Fit a straight line using least squares to the graph of $\log (A_g[\epsilon]/(\epsilon')^2)$ versus $\log (1/\epsilon')$, for $\epsilon' = 2/N, 4/N, \cdots, \epsilon'_{\max}$, where $\epsilon' \triangleq 2\epsilon/N$ is the normalized scale,

$$\frac{2}{N} \leq \epsilon' \leq \epsilon'_{\max} \leq 1 \tag{39}$$

and $\epsilon'_{\max} = 2\epsilon_{\max}/N$. The slope of this line gives us an approximate estimate of the fractal dimension of f, as implied by (32).

Note that when $h = 0$, then step 2 of the algorithm can be done faster; specifically (see also [8] for a more general case),

$$f \oplus_S g[n] = \max \{f[n - 1], f[n], f[n + 1]\}, \qquad \epsilon = 1$$

$$f \oplus_S g^{\oplus(\epsilon+1)}[n] = \max \{f \oplus_S g^{\oplus \epsilon}[n - 1], f \oplus_S g^{\oplus \epsilon}[n + 1]\}, \qquad \epsilon \geq 2. \tag{40}$$

The fractal dimension $D_M(f)$ of the graph of f resulting from the morphological covering method (in both the continuous and discrete case) has the following two attractive properties.

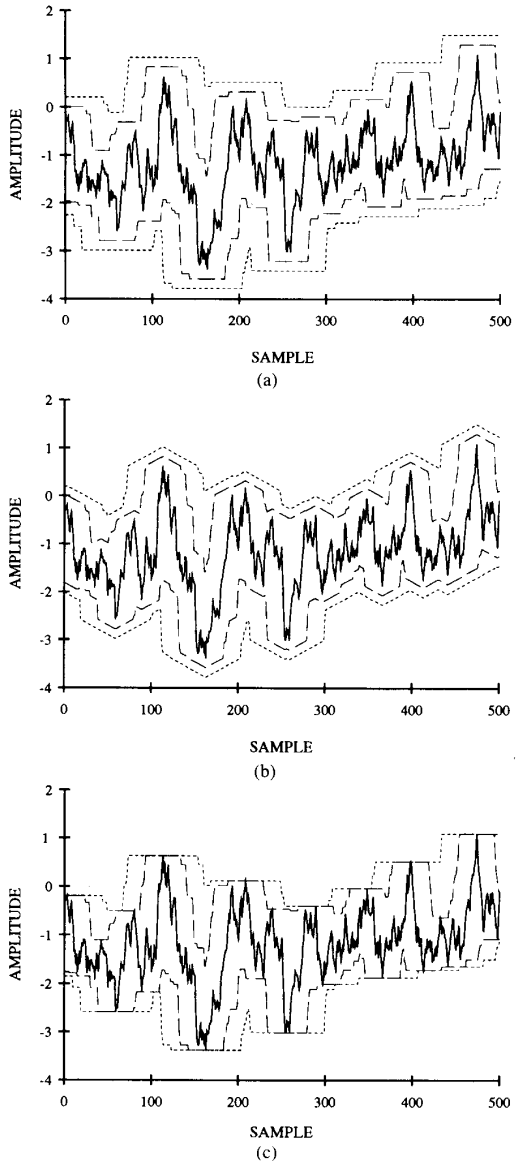

Fig. 2. An FBM signal (solid line) with $D = 1.5$, $N = 500$, and its erosions/dilations (dashed lines) by $g^{\oplus\epsilon}$ at scales $\epsilon = 20, 40$. (a) Rectangular $g = g_r$ with $h = 0.01$. (b) Triangular $g = g_t$ with $h = 0.01$. (c) Rectangular g with $h = 0$.

Property 1: If f is shifted with respect to its argument and/or amplitude, then $D_M(f)$ remains unchanged; i.e., $D_M(f) = D_M(f')$ where $f'(x) = f(x - x_0) + b$.

Property 2: If $h = 0$, then $D_M(f)$ remains invariant with respect to any affine scaling of the amplitude of f and/or shifting of its argument; i.e., $D_M(f) = D_M(f')$ where $f'(x) = af(x - x_0) + b$ for arbitrary b, x_0 and $a \neq 0$.

Proof: The above two properties follow from the fact that morphological erosions and dilations of a signal f by a function g are invariant with respect to constant shifts in the argument and/or the amplitude of f. Further, if $h = 0$, i.e., if g is rectangular and zero on its support, then an affine scaling $f(x) \mapsto af(x)$ will multiply the function-cover area A_g by the factor $|a|$. This factor does not affect the limit in (31) because $\lim_{\epsilon \to 0} \log(|a|/\epsilon) = 0$. Similarly, the factor $|a|$ will only add a constant $\log(|a|)$ in the log-log relation of (32) which does not affect its slope. □

The morphological covering and the box counting method give identical fractal dimension for continuous-time signals f. However, in the discrete case they correspond to different algorithms with different performances. In the discrete case, it is because of Properties 1 and 2 that the morphological covering method is more robust than the box counting method. The latter is affected by arbitrary shifts of the argument of f, by adding constant offsets to f, and (more seriously) by scaling its amplitude range, because all these affect the number of grid boxes intersected by the graph of f. In addition, as noted in [20], the box counting dimension (as well as the morphological method using covers with two-dimensional discrete sets) greatly depends on the relationship between the grid spacing and the dynamic range of f. However, the morphological covering method using covers with one-dimensional functions g can become completely independent from affine scalings of the signal's range if we choose $h = 0$.

Among previous approaches, the one-dimensional version of the work in [32], [37], and [33] corresponds to the morphological covering method using g_t with $h = 1$. The "horizontal structuring element method" in [41], [8] corresponds to using $h = 0$. For "real-world" signals with some fractal structure, the assumption of having the same fractal dimension at all scales may not be true, since the assumption of the same structure existing over all scales is more of a mathematical idealization. Hence, as in [32], many researchers follow the heuristic approach of estimating a profile of local fractal dimension, which for each ϵ is equal to the slope of a line segment fitted via least squares to the log-log plot of (32) over a moving window of a few scales (typically less than ten). In this paper, however, since we are dealing with synthetic signals of a known fractal dimension that is supposed to be constant over all scales, we only compute a single global fractal dimension.

In the rest of this section we explore various numerical issues related with the morphological discrete covering algorithm, its complexity, and its performance on signals synthesized from WCF's, FIF's, and FBM.

Table I compares the computational complexity of the discrete covering algorithm between the cases when g is zero on its support ($h = 0$) versus a nonzero g ($h > 0$). Thus, if we assume that additions and min/max comparisons have roughly the same complexity and if N, $\epsilon_{\max} \gg 1$, then the covering algorithm using $h > 0$ has a complexity $O(8N\epsilon_{\max})$, whereas using $h = 0$ requires a complexity $O(4N\epsilon_{\max})$ which is 50% smaller. Note that the above algorithm which uses function-cover areas A_g has a linear complexity $O(N\epsilon_{\max})$ with respect to the signal's length, whereas using set-cover areas with two-di-

TABLE I
COMPLEXITY OF MORPHOLOGICAL COVERING ALGORITHM

Height of g	$h > 0$	$h = 0$
Additions for cover area A_g	$(2N + 1)\epsilon_{max}$	$(2N + 1)\epsilon_{max}$
Additions for erosions/dilations	$2(N + 1)\epsilon_{max}$	0
Min/Max comparisons for erosions/dilations	$4N\epsilon_{max}$	$2(N - 1)\epsilon_{max} + 2N + 2$

mensional sets has a quadratic complexity $O(N^2\epsilon_{max})$; further, both approaches give the same dimension, as Theorem 1 implies.

Although the shape of the structuring function g is not very crucial, its height h, however, plays an important role. Although h does not affect the morphological covering method in the continuous case, in the discrete case large h will sample the plot of (32) very coarsely and produce poor results. Thus small h are preferred for finer multiscale covering area distributions. However, the smaller h is, the more computations are needed to span a given signal's range. A good practical rule is to set h approximately equal to the signal's dynamic range divided by the number of its samples. This rule attempts to consider the quantization grid in the domain and range of the function as square as possible. We experimentally observed in [26] that this rule performs very similarly to the case $h = 0$, although it gives slightly lower estimates of D. Since, however, for the case $h = 0$, the erosions/dilations by g can be performed faster and the resulting dimension is invariant to affine scalings of the signal's range, we henceforth set $h = 0$ in all our experiments.

The maximum scale ϵ_{max} and in general the scale interval $[1, \epsilon_{max}]$ over which we attempt to fit a line to the log-log plot of (32) is an important parameter. We have experimentally found that the ϵ_{max} required for a good estimation of D may exhibit considerable variations and depends on the dimension D, on the signal's length N, and on the specific class of fractal signals. A heuristic rule for determining ϵ_{max} that we used based on experimental observations is the following:

$$\epsilon_{max} = \text{MaxScale}\ (D, N) = \min\left[\max\left(\frac{(D - 1.2)N}{1.5}, 10\right), \frac{N}{2}\right]. \quad (41)$$

Thus, to apply the morphological covering method to a signal, we have adopted a two-pass procedure which we use in all experiments in this paper. Specifically, we first apply the covering method with $\epsilon = 10$, i.e., a very small scale interval and obtain some estimate D_1 of the fractal dimension. Then we reapply the covering method on the same signal by using $\epsilon_{max} = \text{MaxScale}\ (D_1, N)$ and we obtain a second estimate which we consider as the final estimate D^* of D.

Tables II and III show the estimated dimension D^* and the percent estimation error $100 \cdot |D - D^*|/D$ using the above two-pass covering method on signals with $N + 1 = 501$ samples synthesized from sampling WCF's and FIF's of various D. The WCF's were defined for $t \in [0, 1]$ with $\gamma = 5$. The FIF's interpolated the 6-point data sequence 0, 1, 4, 2, 5, 3 using positive scaling ratios $V = 5^{D-2}$. The experimental results from Tables II and III indicate that, for these two classes of fractal signals, the morphological covering method performs very well in estimating dimensions $D \in [1.2, 1.8]$ with an error of less than 3%. By varying the signals' length $N \in [100, 2000]$ we have also observed similar performance of this method as in varying their dimension. Over 27 different combinations of (D, N) the average percent estimation error of the morphological covering method was 2%–3% for both WCF's and FIF's.

TABLE II
MORPHOLOGICAL COVERING METHOD ON WCF'S

True D	Estimated	Error
1.2	1.227	2.27%
1.3	1.327	2.06%
1.4	1.424	1.71%
1.5	1.515	1.03%
1.6	1.606	0.39%
1.7	1.701	0.03%
1.8	1.797	0.14%

TABLE III
MORPHOLOGICAL COVERING METHOD ON FIF'S

True D	Estimated	Error
1.2	1.204	0.31%
1.3	1.287	0.97%
1.4	1.384	1.12%
1.5	1.478	1.45%
1.6	1.576	1.53%
1.7	1.678	1.29%
1.8	1.782	1.01%

Table IV shows the results from applying the (two-pass) morphological covering method as well as the power spectrum method on FBM signals. For each method and for each true D, the table reports the sample mean D^* of the estimates, the standard deviation, and the percent mean estimation error $100 \cdot |D - D^*|/D$, by averaging results over 100 random FBM realizations. All FBM signals had $N + 1 = 512$ samples and were synthesized using a 512-point FFT. For the power spectrum method, the dimension D was estimated from the slope of a line fitted to the power spectrum of the FBM over the frequency interval $(0, \pi)$. In addition to the (no noise) case of clean FBM signals, Table IV also reports how the estimates from the two methods are affected by adding white Gaussian noise to the FBM realizations at various signal-to-ratio ratios (SNR's). The experimental results from Table IV indicate that the morphological covering method performs well on FBM signals without noise in estimating dimensions $D \in [1.2, 1.6]$ with a relative error less than 5%. For this range of D, the power spectrum yields a larger estimation error than the covering method. How-

TABLE IV
MORPHOLOGICAL COVERING AND POWER SPECTRUM METHODS ON FBM

True D	Morphological Mean	Covering St. Dev.	Error	Power Mean	Spectrum St. Dev.	Error
	No Noise					
1.2	1.249	0.051	4.1%	1.252	0.078	4.3%
1.3	1.326	0.065	2.0%	1.368	0.073	5.3%
1.4	1.393	0.057	0.5%	1.437	0.069	2.7%
1.5	1.474	0.058	1.7%	1.544	0.063	2.9%
1.6	1.553	0.046	2.9%	1.653	0.072	3.3%
1.7	1.599	0.048	5.9%	1.753	0.079	3.1%
1.8	1.646	0.033	8.6%	1.825	0.072	1.4%
	SNR = 30 dB					
1.2	1.276	0.050	6.3%	1.493	0.083	24.4%
1.3	1.343	0.062	3.3%	1.520	0.060	16.9%
1.4	1.425	0.057	1.8%	1.563	0.054	11.6%
1.5	1.482	0.050	1.2%	1.622	0.067	8.1%
1.6	1.540	0.046	3.7%	1.681	0.058	5.0%
1.7	1.599	0.039	5.9%	1.773	0.060	4.3%
1.8	1.644	0.036	8.7%	1.842	0.064	2.3%
	SNR = 20 dB					
1.2	1.403	0.040	16.9%	1.769	0.101	47.4%
1.3	1.432	0.043	10.2%	1.758	0.075	35.2%
1.4	1.480	0.039	5.7%	1.752	0.065	25.2%
1.5	1.512	0.041	0.8%	1.753	0.064	16.9%
1.6	1.558	0.040	2.6%	1.783	0.054	11.4%
1.7	1.609	0.037	5.4%	1.842	0.054	8.3%
1.8	1.649	0.034	8.4%	1.891	0.057	5.0%
	SNR = 10 dB					
1.2	1.600	0.024	33.4%	2.075	0.080	72.9%
1.3	1.602	0.026	23.3%	2.065	0.073	58.9%
1.4	1.616	0.024	15.4%	2.041	0.068	45.8%
1.5	1.621	0.025	8.0%	2.007	0.066	33.8%
1.6	1.638	0.023	2.4%	2.006	0.056	25.4%
1.7	1.663	0.026	2.2%	2.014	0.047	18.5%
1.8	1.685	0.025	6.4%	2.027	0.052	12.6%

ever, for higher dimensions $D \in (1.6, 1.8]$ the covering method almost always underestimates the true D and its estimation error increases to about 5%–10%, whereas the power spectrum method overestimates D but with a smaller error. As we start adding noise the performance of both methods deteriorates, with D's less than 1.5 affected much more than D's above 1.5. In noise, the performance of the power spectrum method deteriorates more rapidly than that of morphological covering. Especially for SNR $\leq$ 10 dB the power spectrum method yields D estimates which are completely wrong because they often exceed the allowable range [1, 2]. Finally, the standard deviation of the morphological covering method appears to be almost always smaller than that of the power spectrum method for almost all D and SNR's. Regarding all the above issues, we have also observed similar behavior of both methods while varying the signals' length $N + 1 \in \{2^7, 2^8, 2^9, 2^{10}, 2^{11}\}$. Some conclusions from all these extensive experimental results are summarized by Table V, which provides the sample mean percent estimation error of both the morphological covering and the power spectrum method, averaged over 7×5 combinations of (D, N) with 100 random FBM realizations each. There we see that in the absence of noise, both methods yield a similar average error of about 3%–4%, whereas in the presence of noise the morphological covering method yields much smaller error. Thus, overall the morphological covering method appears to be a more robust method to estimate the dimension of an FBM signal for most values of D, N, and SNR.

TABLE V
AVERAGE PERCENT ERROR IN ESTIMATING THE DIMENSION OF FBM

	Morphological Covering	Power Spectrum
No noise	3.8%	3.6%
SNR = 20 dB	7.7%	22.3%

Concluding, we emphasize that, since all three classes of fractal signals are sampled versions of non-band-limited fractal functions, some degree of fragmentation is irreversibly lost during sampling. Hence, since the true D refers to the continuous-time signal, the discrete morphological covering algorithm (as well as any other discrete algorithm) can offer only an approximation of D. In addition, the specific approach used to synthesize the discrete fractal signals (e.g., the FFT for FBM) affects the relationship between the degree of their fragmentation and the true D, and hence it may also affect the performance of the D estimation algorithms.

IV. ITERATIVE OPTIMIZATION METHOD

Assume a class of deterministic fractal signals f_P parameterized by a parameter P that is related to their fractal dimension through an invertible function $D = \psi(P)$. For

example, for WCF's the parameter P is H and $D = \psi(H) = 2 - H$. For FIF's that interpolate a $N + 1$-point sequence using a constant scaling ratio $V > 0$, the parameter P is V and $D = \psi(V) = 2 + \log(V)/\log(K)$. Since P and D are in one-to-one correspondence, we can henceforth parameterize the signal using D. Our new approach to measure the fractal dimension of such a signal f_D consists of the following steps: 1) We use a simple and fast morphological approach, i.e., the two-pass covering method with $h = 0$, to come up with an initial estimate D^* of the true D. 2) We compute some distance between the original fractal signal f_D and another signal f_{D^*}, which was synthesized to have dimension exactly D^*. 3) By using simple nonlinear optimization techniques, we search in the parameter space of D values of the chosen class of fractals by synthesizing fractals with fractal dimension D^* and computing their distances from the original fractal until this cycle converges to a minimum in the parameter space. In this way the resulting fractal dimension will correspond to a fractal signal which is also close (with respect to the specific distance) to the original signal. We call this the iterative optimization method. As distances we have used the standard l_p metrics

$$l_p(f_1, f_2) \triangleq \begin{cases} \left(\sum_{n=-\infty}^{\infty} |f_1[n] - f_2[n]|^p \right)^{1/p}, \\ \qquad p = 1, 2, \cdots \\ \max_n \{|f_1[n] - f_2[n]|\}, \qquad p = \infty \end{cases} \tag{42}$$

as well as the Hausdorff metric. The Hausdorff metric was so far defined only for sets. Here we extend its definition to signals and provide a morphological algorithm for its computation. Given two compact sets S_1, S_2 their Hausdorff distance can be computed as

$$\text{dist}_H(S_1, S_2) \triangleq \inf \{\epsilon \geq 0: S_1 \subseteq S_2 \oplus \epsilon B \text{ and } S_2 \subseteq S_1 \oplus \epsilon B\} \tag{43}$$

where ϵB is a disk of radius ϵ. Let f_1, f_2 be two discrete-time signals with finite length, and let g be a structuring function equal either to g_r or g_t defined in (35), (36) with $h > 0$. Then we define the Hausdorff distance between f_1 and f_2 by

$$\text{Hy}(f_1, f_2) \triangleq \min \{\epsilon: f_1 \leq f_2 \oplus g^{\oplus \epsilon} \text{ and } f_2 \leq f_1 \oplus g^{\oplus \epsilon}\} \tag{44}$$

where $\epsilon \geq 0$ takes only integer values and $f_1 \leq f_2$ denotes the function ordering $f_1[n] \leq f_2[n]$ $\forall n$. Note that $\text{Hy}(f_1, f_2)$ is equal to dist_H [Ypo(f_1), Ypo(f_2)], where the set $\text{Ypo}(f) = \{(t, y) \in \mathbb{R}^2: y \leq f(t)\}$ is the hypograph of f (also known as "umbra" in mathematical morphology) and the disk-like set B needed for $\text{dist}_H(,)$ is related to g. It is simple to show that Hy satisfies all formal requirements for being a distance metric. Hy compares f_1 and f_2 in terms of their peaks (i.e., graph protrusions). Our motivation for using this Hausdorff distance is that it is better suitable than l_p distances for certain applications, i.e., for matching two shapes based on their protrusions and/or indentations [31].

Of course, the effectiveness of the iterative optimization method depends on the possible existence of a global minimum in the distances over the parameter space. Figs. 3 and 4 report a series of experiments whose goal was to investigate how well the l_1 and Hausdorff distances can find a global minimum in comparing a given parametric fractal with an ensemble of similar fractals whose parameter varies over all possible values. Fig. 3 shows the distances between WCF's, and Fig. 4 shows the same distances for FIF's. These figures illustrate that both the l_1 and the Hy distance yield a very clear global minimum when comparing an original WCF or FIF signal of a fixed D with similar signals whose D^* spans all of the interval (1, 2). (In Figs. 3 and 4, only the results for $D^* \in (1, 1.9]$ are shown because higher D^* yields very large distances.) This global minimum exists independently of D or N. Resolutions of anywhere between 0.01 and 0.1 suffice to sample the parameter space of D and still observe a clear minimum. We have also examined the l_2 and l_∞ distances, and they all had similar performance in yielding a clear global minimum in the distance function for signals produced by both WCF's and FIF's.

The following theorem establishes the existence of the observed global minimum for all the above distances.

Theorem 3: Let $E(D^*) = \text{dist}(f_D, f_{D^*})$ be the distance function between two signals f_D and f_{D^*} from the same parametric fractal class, one with arbitrary but fixed dimension $D \in (1, 2)$ and the other with variable dimension $D^* \in (1, 2)$, where dist (,) is any of the l_p or Hausdorff distances. Then E has a global minimum at $D^* = D$ for the following types of parametric fractals: a) signals resulting from sampling WCF's over any time interval, and b) signals resulting from sampling FIF's that interpolate any nonnegative (respectively, nonpositive) finite sequence using a positive (respectively, negative) constant vertical scaling ratio V.

Proof: a) Let us index the WCF W_H of (7) in terms of D, and let the discrete fractal signal f_D be a sampled version of W_D. Then for each $D_1 = 2 - H_1$ and $D_2 = 2 - H_2$ we have

$$D_1 \leq D_2 \Rightarrow W_{D_1}(t) \leq W_{D_2}(t) \qquad \forall t \tag{45}$$

because $\gamma^{-kH_1} \leq \gamma^{-kH_2}$ for all $k \geq 0$. This pointwise monotonic ordering of $W_D(t)$ with D at each t creates a similar monotonic ordering in the distances between their sampled versions f_D; i.e.,

$$D_2 \leq D_1 \leq D \Rightarrow \text{dist}(f_D, f_{D_1}) \leq \text{dist}(f_D, f_{D_2})$$
$$D \leq D_3 \leq D_4 \Rightarrow \text{dist}(f_D, f_{D_3}) \leq \text{dist}(f_D, f_{D_4}) \tag{46}$$

where dist (,) is any of the l_p or Hausdorff distances. For a fixed D, this creates a global minimum in dist (f_D, f_{D^*}) at $D^* = D$.

b) Let F_{D_1} and F_{D_2} be two FIF's, indexed by their fractal dimensions D_1, D_2, that interpolate the same sequence

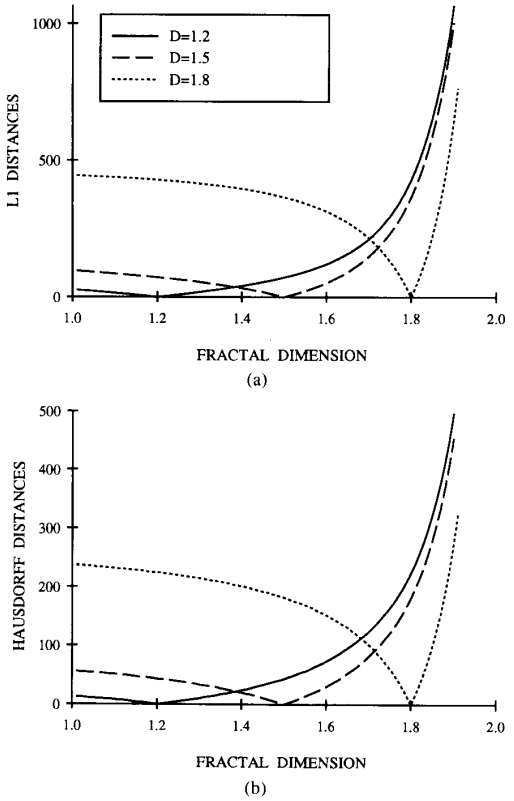

Fig. 3. (a) Distances $l_1(W_D, W_{D^*})$ between three fixed signals W_D synthesized by sampling WCF's with $D = 1.2, 1.5, 1.8$ and variable WCF signals W_{D^*} whose D^* spans the interval [1.01, 1.90] at steps of 0.01. (b) The same as (a) but using Hausdorff distances with $g = g_l$ and $h = 0.01$. (All WCF's are defined over [0, 1] with $\gamma = 5$; $N = 500$.)

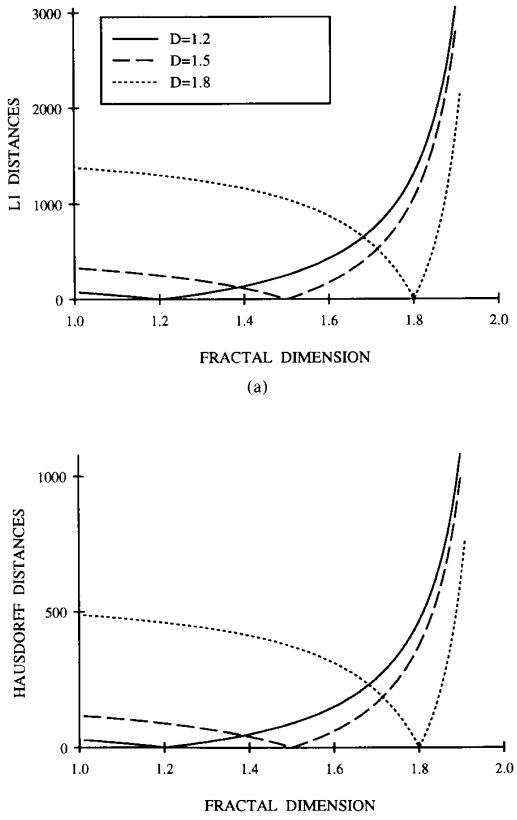

Fig. 4. (a) Distances l_1 (F_D, F_{D^*}) between three fixed signals F_D synthesized by sampling FIF's with $D = 1.2, 1.5, 1.8$ and variable FIF signals F_{D^*} whose D^* spans the interval [1.01, 1.90] at steps of 0.01. (b) The same as (a) but using Hausdorff distances with $g = g_l$ and $h = 0.01$. (All FIF's correspond to interpolating the sequence 0, 1, 4, 2, 5, 3 with $N = 500$ and $V = 5^{D-2}$.)

$\{(x_k, y_k): k = 0, 1, \cdots, K\}$ using constant scaling ratios $V_1 = \pm K^{D_1 - 2}$ and $V_2 = \pm K^{D_2 - 2}$. Let Ψ_1, Ψ_2 be their corresponding contraction mappings (9) defined on $\mathcal{Q}$. Define the function $q \in \mathcal{Q}$ to be equal to the piecewise-linear interpolant of the (x_k, y_k) data. Assume now that all $y_k \geq 0$, which makes q a nonnegative function, and select $V_1, V_2 > 0$. If $D_1 \leq D_2$, it follows from (13) that $V_1 \leq V_2$; then from (9) it follows that $\Psi_1(q) \leq \Psi_2(q)$. (We will arrive at the same conclusion if we assume all $y_k \leq 0$ and $V_1, V_2 < 0$, because then q is a nonpositive function and $V_1 q \leq V_2 q$.) Since $F_{D_j} = \lim_{n \to \infty} \Psi_j^{on}(q)$, $j = 1, 2$, we obtain the final result

$$D_1 \leq D_2 \Rightarrow F_{D_1}(t) \leq F_{D_2}(t) \qquad \forall t \in [x_0, x_K]. \quad (47)$$

This pointwise monotonic ordering of FIF's $F_D(t)$ with D at each t creates a monotonic ordering in the distances between their sampled versions f_D exactly as in (46) for the WCF case, from which the proof of b) follows. □

Theorem 3 guarantees the convergence of the iterative optimization method to the true D using any of the l_p or Hausdorff distances. Tables VI and VII show the estimated dimension using the iterative optimization method and the percent estimation error for signals stemming from WCF's and FIF's with variable dimension and fixed

TABLE VI
ITERATIVE OPTIMIZATION METHOD ON WCF's

True D	Estimated	Error
1.2	1.2003	0.02%
1.3	1.2998	0.01%
1.4	1.4000	0.00%
1.5	1.5004	0.03%
1.6	1.6012	0.07%
1.7	1.6996	0.02%
1.8	1.8004	0.02%

TABLE VII
ITERATIVE OPTIMIZATION METHOD ON FIF'S

True D	Estimated	Error
1.2	1.1998	0.02%
1.3	1.3004	0.03%
1.4	1.4003	0.02%
1.5	1.5002	0.02%
1.6	1.5996	0.03%
1.7	1.7001	0.01%
1.8	1.7997	0.01%

length. (The signal parameters are the same as for the Tables II and III.) The iterative optimization was implemented by using the initial estimate from the two-pass morphological covering method (with $h = 0$), and then improving it by first proceeding in the D space at steps of OS = 0.01 and then (when in the neighborhood of the global minimum) by refining it with optimization steps of OS/10. The convergence of these iterations was relatively fast, i.e., in the order of 10–30 iterations. The small number of iterations can be approximately predicted by considering that the initial estimate from the morphological covering method yields an error of approximately no more than 10%, corresponding to an actual D estimation error of no more than 0.2; this in turn causes the iterative optimization method to require about $0.2/\mathrm{OS} \approx 20$ iterations to reach the true value of D. The experimental results reported in Tables VI and VIII show that the iterative optimization method gave extremely good estimates of D with errors of 0.07% or less. Actually the errors are generally guaranteed to be in the order of OS/10; they can also be driven down to practically zero by selecting a finer optimization step at the expense of more iterations. The l_1 distance was used, but the Hy distance performed very similarly. The same conclusions were also reached by experimenting with signals with variable duration $N \in [100, 2000]$ and fixed dimension.

So far we have seen the iterative optimization method working for deterministic parametric fractals. For random parametric fractals, such as the FBM signals, the distances are random variables and we need to compare their mean value. In an earlier work [26] we found that, if we use the same seed (for the random generator underlying the FFT-based synthesis algorithm) for the FBM signal with fixed D and all the other FBM signals with varying D^*, then their sample mean distance has a global minimum, which enables the iterative optimization method to work successfully. Note, however, that using the same seed implies that the collection of FBM signals with different D^* is not completely random since the overall shape of the signals would be preserved and only their fractal roughness would vary with D^*. In the general case, when we change the seed corresponding to the FBM signals with varying D^*, we found that there is not a clear minimum in the mean distance and hence the iterative optimization method does not work successfully in this case.

Finally, we have seen the excellent performance of the iterative optimization method on deterministic fractals such as WCF's and FIF's under a variety of distances such as l_p and Hausdorff distances. For signals of N samples the l_1 distance has $O(N)$ computational complexity. If we divide the range of the signals into about N cells of spacing h, where h is the height of the structuring function g used in the computation of Hy, then the Hausdorff distance Hy has complexity $O(N^2)$. However, despite the fact that the Hy distance has a higher computational complexity than l_1 while both yield similar results, we think that the Hausdorff distance is useful for several applications. For example, it has been found that for shape matching [31] or for approximating a fractal signal with a fractal interpolation function [26], Hy is more suitable than l_p distances to compare the shape of two signals in terms of their overall geometrical structure, which is a signal attribute that fractal methods attempt to capture.

V. Conclusions

We have developed a theoretical approach for measuring the fractal dimension of arbitrary continuous-time signals by using morphological erosion and dilation function operations to create covers around a signal's graph at multiple scales. A related algorithm has also been developed for discrete-time signals. This morphological covering approach unifies and extends the theoretical aspects and digital implementations of several other covering methods, and it also has some computational advantages. Its computational complexity is linear with respect to both the signal's length and the maximum scale. It has a good performance, since it has experimentally been found to yield average estimation errors (averaged over many different signal dimensions and lengths) of about 2%–4% or less for discrete fractal signals synthesized from Weierstrass functions, fractal interpolation functions, and fractal Brownian motion.

For deterministic fractal signals (e.g., Weierstrass and fractal interpolation functions) depending on a single parameter that uniquely corresponds to their fractal dimension, we have also developed an optimization method that starts from an initial estimate and iteratively converges to the true fractal dimension by minimizing a distance between the original signal and all such signals from the same class. This iterative optimization method has an excellent performance, since it has been both theoretically and experimentally found to yield practically zero estimation errors using either l_p or Hausdorff signal distances.

References

[1] M. F. Barnsley, "Fractal interpolation," *Constr. Approx.*, vol. 2, pp. 303–329, 1986.

[2] M. F. Barnsley, *Fractals Everywhere*. New York: Academic, 1988.

[3] R. G. Bartle, *The Elements of Real Analysis*. New York: Wiley, 1976.

[4] M. V. Berry and Z. V. Lewis, "On the Weierstrass-Mandelbrot fractal function," *Proc. Roy. Soc., Ser. A*, vol. 370, pp. 459–484, 1980.

[5] A. S. Besicovitch, "On the sum of digits of real numbers represented in the dyadic system (On sets of fractional dimension—II)," *Math. Annalen*, vol. 110, pp. 321–329, 1934; also "Sets of fractional dimension—IV: On rational approximation to real numbers," *J. London Math. Soc.*, vol. 9, pp. 126–131, 1934.

[6] A. S. Besicovitch and H. D. Ursell, "Sets of fractional dimension—V: On dimensional numbers of some continuous curves," *J. London Math. Soc.*, vol. 12, pp. 18–25, 1937.

[7] G. Bouligand, "Ensembles impropres et nombre dimensionnel," *Bull. Sci. Math.*, vol. II-52, pp. 320–344, 361–376, 1928; also in *Bull. Sci. Math*, vol. II-53, pp. 185–192, 1929.

[8] B. Dubuc, J. F. Quiniou, C. Roques-Carmes, C. Tricot, and S. W. Zucker, "Evaluating the fractal dimension of profiles," *Phys. Rev. A*, vol. 39, pp. 1500–1512, Feb. 1989.

[9] K. Falconer, *Fractal Geometry: Mathematical Foundations and Applications*. New York: Wiley, 1990.

[10] J. D. Farmer, E. Ott, and J. A. Yorke, "The dimension of chaotic attractors," *Physica 7D*, pp. 153–180, 1983.

[11] R. M. Haralick, S. R. Sternberg, and X. Zhuang, "Image analysis

using mathematical morphology," *IEEE Trans. Patt. Anal. Machine Intell.*, vol. PAMI-9, pp. 523-550, July 1987.
[12] D. P. Hardin and P. R. Massopust, "The capacity for a class of fractal functions," *Commun. Math. Phys.*, vol. 105, pp. 455-460, 1986.
[13] G. H. Hardy, "Weierstrass's nondifferentiable function," *Trans. Amer. Math. Soc.*, vol. 17, pp. 322-323, 1916.
[14] F. Hausdorff, "Dimension and ausseres Mass," *Math. Annalen*, vol. 79, pp. 157-179, 1918.
[15] H. J. A. M. Heijmans and C. Ronse, "The algebraic basis of mathematical morphology—Part I: Dilations and erosions," *Comput. Vision, Graphics, Image Processing*, vol. 50, pp. 245-295, 1990.
[16] J. Hutchinson, "Fractals and self-similarity," *Indiana Math. J.*, 1981.
[17] A. N. Kolmogorov and V. M. Tihomirov, "Epsilon-entropy and epsilon-capacity of sets in functional spaces," *Usp. Matematicheskikh Nauk. (N.S.)*, vol. 14, pp. 3-86, 1959 (translated in *Trans. Amer. Math. Soc.*, (ser. 2) vol. 17, pp. 277-364, 1961).
[18] T. Lundahl, W. J. Ohley, S. M. Kay, and R. Siffert, "Fractional Brownian motion: A maximum likelihood estimator and its application to image texture," *IEEE Trans. Med. Imaging*, vol. MI-5, pp. 152-160, Sep. 1986.
[19] B. B. Mandelbrot, *The Fractal Geometry of Nature*. New York: Freeman, 1982/1983.
[20] B. B. Mandelbrot, "Self-affine fractals and fractal dimension," *Phys. Scripta*, vol. 32, pp. 257-260, 1985.
[21] B. B. Mandelbrot and J. van Ness, "Fractional Brownian motion, fractional noise, and applications," *SIAM Rev.*, vol. 10, no. 4, pp. 422-437, 1968.
[22] B. B. Mandelbrot and J. R. Wallis, "Computer experiments with fractional Brownian motion—Parts 1-3," *Water Resources Res.*, vol. 5, pp. 228-267, Feb. 1969.
[23] P. Maragos, "Fractals aspects of speech signals: Dimension and interpolation," in *Proc. IEEE ICASSP-91*, Toronto, Canada, May 1991.
[24] P. Maragos and R. W. Schafer, "Morphological filters—Part I: Their set-theoretic analysis and relations to linear shift-invariant filters," *IEEE Trans. Acoust., Speech, Signal Processing*, vol. ASSP-35, pp. 1153-1169, Aug. 1987.
[25] P. Maragos and R. W. Schafer, "Morphological systems for multidimensional signal processing," *Proc. IEEE*, vol. 78, pp. 690-710, Apr. 1990.
[26] P. Maragos and F. K. Sun, "Measuring fractal dimension: Morphological estimates and iterative optimization," in *Proc. SPIE Int. Soc. Opt. Eng.*, vol. 1199, pp. 416-430, 1989.
[27] D. S. Mazel and M. H. Hayes, III, "Hidden-variable fractal interpolation of discrete sequences," in *Proc. IEEE ICASSP-91*, Toronto, Canada, May 1991.
[28] C. McMullen, "The Hausdorff dimension of general Sierpinski carpets," *Nagoya Math. J.*, vol. 96, pp. 1-9, 1984.
[29] P. Meakin, "Diffusion-controlled cluster formation in 2-6 dimensional space," *Phys. Rev. A*, vol. 23, no. 3, pp. 1495-1507, 1983.
[30] H. Minkowski, "Uber die Begriffe Lange, Oberflache und Volumen," *Jahresber. Deutch. Mathematikerverein.*, vol. 9, pp. 115-121, 1901.
[31] D. Mumford, "The problem of robust shape description," in *Proc. 1st Int. Conf. Comput. Vision*, London, U.K., 1987.
[32] S. Peleg, J. Naor, R. Hartley, and D. Avnir, "Multiple resolution texture analysis and classification," *IEEE Trans. Patt. Anal. Machine Intell.*, vol. PAMI-6, pp. 518-523, July 1984.
[33] T. Peli, V. Tom, and B. Lee, "Multiscale fractal and correlation signatures for image screening and natural clutter suppression," *Proc. SPIE Int. Soc. Opt. Eng.*, vol. 1199, pp. 402-415, 1989.
[34] A. P. Pentland, "Fractal-based description of natural scenes," *IEEE Trans. Patt. Anal. Machine Intell.*, vol. PAMI-6, pp. 661-674, Nov. 1984.
[35] J. Serra, *Image Analysis and Mathematical Morphology*. New York: Academic, 1982.
[36] J. Serra and L. Vincent, "An overview of morphological filtering," *Circuits, Syst., Signal Processing*, vol. 11, no. 1, pp. 47-108, 1992.
[37] M. C. Stein, "Fractal image models and object detection," *Proc. SPIE Int. Soc. Opt. Eng.*, 1987.
[38] S. R. Sternberg, "Grayscale morphology," *Comput. Vision, Graph., Image Processing*, vol. 35, pp. 333-355, 1986.
[39] B. J. Super and A. C. Bovik, "Localized measurement of image fractal dimension using Gabor filters," *J. Visual Commun. Image Represent.*, vol. 2, pp. 114-128, June 1991.
[40] A. H. Tewfik and M. Deriche, "Maximum likelihood estimation of the fractal dimensions of stochastic fractals and Cramer-Rao bounds," in *Proc. IEEE ICASSP-91*, Toronto, Canada, May 1991.
[41] C. Tricot, J. Quiniou, D. Wehbi, C. Roques-Carmes, and B. Dubuc, "Evaluation de la dimension fractale d'un graphe," *Rev. Phys. Appl.*, vol. 23, pp. 111-124, 1988.
[42] R. F. Voss, "Fractals in nature: From characterization to simulation," in *The Science of Fractal Images*, H.-O. Peitgen and D. Saupe, Eds. New York: Springer-Verlag, 1988.
[43] G. W. Wornell and A. V. Oppenheim, "Fractal signal modeling and processing using wavelets," in *Proc. 1990 DSP Workshop*, Mohonk, New Paltz, NY, Sept. 1990.

Petros Maragos (S'81-M'81-SM'91) was born in Kalymnos, Greece, in 1957. He received the Diploma degree in electrical engineering from the National Technical University of Athens, Greece, in 1980, and the M.S.E.E. and Ph.D. degrees from the Georgia Institute of Technology, Atlanta, in 1982 and 1985, respectively.

From 1980 to 1985 he was a Research Assistant at the Digital Signal Processing Lab of the Electrical Engineering School at Georgia Tech. In 1985 he joined the faculty of the Division of Applied Sciences at Harvard University, Cambridge, where he is currently an Associate Professor of Electrical Engineering. During fall 1992 he was a Visiting Professor at the National Technical University of Athens. His general research and teaching activities are in signal processing, computer speech, and computer vision. Some of his current research focuses on morphological signal/image processing, fractal signal/image analysis, and nonlinear modeling of speech production.

Dr. Maragos served as an Associate Editor for the IEEE TRANSACTIONS ON SIGNAL PROCESSING during 1989-1991. He is currently on the Editorial Board for the *Journal of Visual Communication and Image Representation*. He was the Chairman of the SPIE Conference on Visual Communications and Image Processing in Boston, 1992. He received a Sigma Xi Thesis Research Award in 1983; a National Science Foundation Presidential Young Investigator Award in 1987; and the IEEE Acoustics, Speech, and Signal Processing Society's 1988 Paper Award for a publication in the society's transactions.

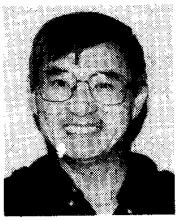

Fang-Kuo Sun (S'71-M'76-SM'86) received the B.S. degree in control engineering from the National Chiao-Tung University, Hsinchu, Taiwan, the M.S. degree in electrical engineering from the University of Pittsburgh, Pittsburgh, PA, in 1972, the M.A. degree in 1976, and the Ph.D. degree in decision and control from Harvard University, Cambridge, MA, in 1976.

He is the founder of Reading Information Technology, Reading, MA. He worked for the Analytic Sciences Corporation, Reading, MA, from 1977 to 1991, and for the Scientific Research Laboratory, Ford Motor Company, Dearborn, MI, from 1976 to 1977. His research interests are in distributed geographic and management information systems; autonomous image analysis; remote sensing and computer vision; and system modeling, evaluation, and performance analysis.

Dr. Sun is a member of SIAM and Sigma Xi and is a Fellow of the SPIE.